JOURNAL OF CATALYSIS 143, 464–480 (1993)

Propene Oxidation over Cu_2O Single-Crystal Surfaces: A Surface Science Study of Propene Activation at 1 atm and 300 K

KIRK H. SCHULZ[1] AND DAVID F. COX[2]

Department of Chemical Engineering, Virginia Polytechnic Institute and State University, Blacksburg, Virginia 24061

Received December 2, 1992; revised May 3, 1993

Propene oxidation was studied on Cu_2O single-crystal surfaces using XPS and TDS in ultrahigh vacuum (UHV) following propene exposures at 300 K and atmospheric pressure. Three different Cu_2O surfaces were examined: a Cu^+-terminated (100) surface, an oxygen-terminated (100) surface, and a (111) surface with accessible copper cations and lattice oxygen. Selective oxidation to acrolein is promoted by coordinately unsaturated surface lattice oxygen. No clear correlation between the formation of partial oxidation products and oxygen coordination was observed. Both selective and nonselective oxidation products are formed from lattice oxygen. The propene oxidation pathway proceeds through an allyloxy (CH_2=$CHCH_2O$–) species where oxygen insertion occurs prior to the second hydrogen abstraction over Cu_2O. This conclusion was reached by comparing the propene TDS results from atmospheric pressure exposures with UHV allyl alcohol and acrolein thermal desorption data. The selective oxidation process over Cu_2O is subject to a "pressure gap" at 300 K with oxygen insertion occurring at higher pressures, presumably because of translational and collisional activation. However, the subsequent steps in the selective oxidation pathway can be effectively modeled by dissociative adsorption of oxygenates under UHV to simulate the oxygenated surface intermediates.

INTRODUCTION

The partial oxidation of propene (CH_2=$CHCH_3$) to acrolein (CH_2=$CHCHO$) is a useful model for the class of allylic oxidation reactions of olefins. Several mixed oxides catalyze propene partial oxidation to acrolein, but Cu_2O is the only reported single-component oxide catalyst to exhibit significant selectivity and activity (*1–3*). There is evidence that some details of the reaction pathway are similar over the bismuth–molybdate (*4*), tin–antimony oxide (*5*), uranium–antimonate (*6*), and single-component Cu_2O catalysts (*4*). Thus, mechanistic information obtained over Cu_2O may be applicable to more complex mixed oxide systems (*2–7*).

The basic steps in the reaction pathway of propene oxidation to acrolein have been widely studied. In the rate-determining step over Cu_2O and bismuth–molybdate catalysts, a methyl (i.e., allylic) hydrogen is abstracted from propene producing a symmetric π-allyl intermediate (*4, 8*). The order in which the final two reaction steps occur is not well understood, but involves a second hydrogen abstraction and lattice oxygen insertion into the symmetric π-allyl to form an oxygen-containing, σ-allyl species. Grasselli and Burrington (*3*) advocate the formation of a σ-allyl on bismuth-molybdate catalysts where oxygen insertion occurs *prior* to the final (second) hydrogen abstraction (i.e., an allyloxy intermediate, CH_2=$CHCH_2O$–). However, in earlier studies several groups advocated the formation of a σ-allyl species on bismuth–molybdate (*1*) and Cu_2O (*7*) catalysts where lattice oxygen insertion occurs *after* the final hy-

[1] Current address: University of North Dakota, Department of Chemical Engineering, Box 8101, University Station, Grand Forks, ND 58202.

[2] To whom correspondence should be addressed.

0021-9517/93 $5.00

drogen abstraction (i.e., an oxygen-containing intermediate with a composition identical to that of acrolein).

Propene oxidation over Cu_2O catalysts has been widely studied over the past several decades (*4–7, 9*). Mikhal'chenko *et al.* studied propene adsorption and oxidation over Cu_2O powders. They proposed two different forms of adsorbed propene on Cu_2O: a reversibly adsorbed and an irreversibly adsorbed propene species (*10, 11*). The reversibly adsorbed propene formed partial oxidation products, while the irreversibly adsorbed propene formed CO_2 and H_2O (*11*). A continuation of these studies using IR suggested that acrolein was formed from propene through allyl complexes on Cu_2O (*10*). In a more recent investigation, Davydov *et al.* used IR to study propene adsorption on Cu_2O and mixed copper oxide–magnesium oxide catalysts (*12*). They observed both π- and σ-allyl species on Cu_2O following propene adsorption, and suggest that the π-allyl species is stable to between 523 and 573 K, whereas the σ-allyl is stable to about 373 K. The assignment of a π-allyl species was made via the C=C stretch at 1510 cm^{-1} by comparison with the IR spectra of π-complexes of propene with metals. Davydov *et al.* also suggested that propene forms acrolein through an allyloxy species (CH_2=$CHCH_2O$–).

Imachi *et al.* studied the reactions of deuterium-labeled propene over Cu_2O with microwave spectroscopy (*13*). They observed a primary kinetic isotope effect for the production of two different forms of acrolein from CH_3CH=CHD. This observation leads to the suggestion that conversion from a π-allyl to a σ-allyl from adsorbed propene is not reversible, and that once the σ-allyl species is formed it does not readily convert to a σ-allyl isomer or a π-allyl.

Choi *et al.* examined the reaction of ^{18}O-labeled allyl alcohol over supported Cu_2O (*9*). They observed a partial loss of the ^{18}O in the product acrolein, illustrating that some scission of the C–O bond and reoxidation by surface oxygen had occurred. Choi and coworkers also suggest that the σ-allyl intermediate formed from allyl alcohol is similar to the σ-allyl formed during acrolein production from propene. Further, their results suggest that the oxygen-containing σ-allyl is not in equilibrium with a π-allyl under reaction conditions.

Wood *et al.* studied propene oxidation over low-surface-area, unoriented, Cu_2O crystals as a function of surface condition (*14*). They found that copper-rich Cu_2O tends to favor acrolein production, while oxygen-rich Cu_2O favors CO_2 and H_2O production. Results from supported copper oxide catalysts have shown that Cu_2O favors partial oxidation products, while CuO favors nonselective oxidation products (*15*).

Propene adsorption has been studied previously on Cu_2O single crystal surfaces under low pressure (10^{-4} Torr) and ultrahigh vacuum (UHV) conditions (*16*). No C_3 partial oxidation products were detected for propene adsorption between 100 and 300 K. However, evidence for propene dissociation to an allyl (C_3H_5) was observed after adsorption at 300 K on both the $Cu_2O(100)$ and (111) surfaces. Also, propene dissociation to allyl was observed in the presence of oxygen vacancies on the (111) surface following adsorption at 110 K. No determination could be made from the thermal desorption and photoemission data concerning the nature of the C_3H_5 allyl species (i.e., π- or σ-allyl). A complete description of these results is given elsewhere (*16*).

SURFACES INVESTIGATED

The use of Cu_2O single crystal surfaces as model catalysts allows for the testing of site requirements for propene adsorption and oxidation. The two low-index surfaces investigated differ both in the availability of surface lattice oxygen and the Cu^+ coordination numbers. The ideal, stoichiometric, nonpolar, $Cu_2O(111)$ surface exposes singly and doubly coordinate Cu^+ cations (bulk Cu^+ coordination = 2) in the second atomic layer in a ratio of 1 to 4, respectively. However, the top atomic layer is composed ex-

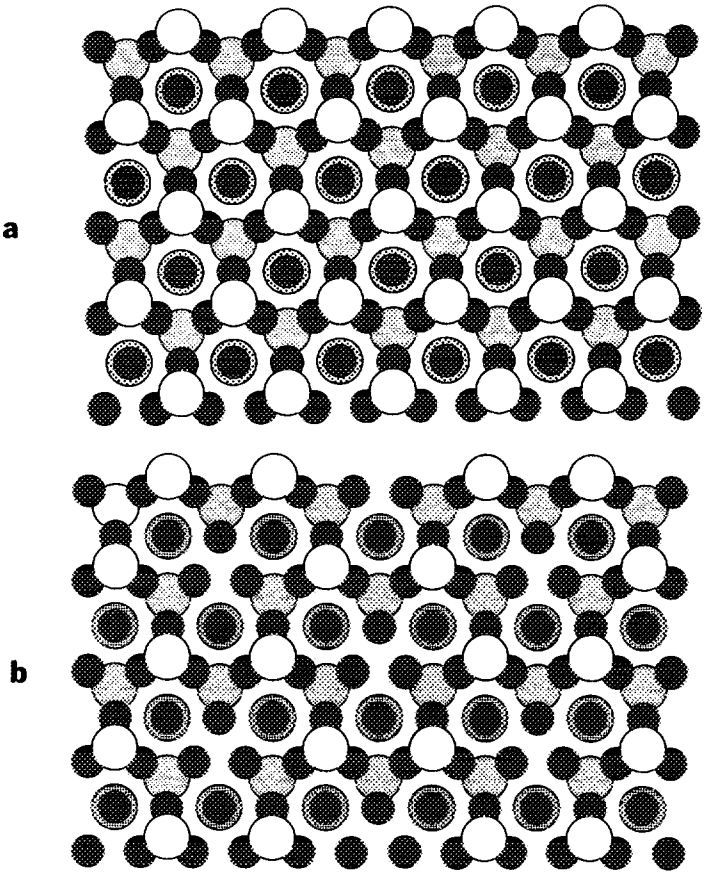

FIG. 1. Ball model illustrations of (a) the ideal, stoichiometric $Cu_2O(111)$ surface and (b) the oxygen-deficient $Cu_2O(111)$-$(\sqrt{3} \times \sqrt{3})R30°$ surface. The small filled circles represent Cu^+ cations, and the larger open circles represent O^{2-} anions. For clarity, only the top four atomic layers are shown. The illustrations assume no surface relaxation.

clusively of threefold-coordinate oxygen anions (bulk lattice O^{2-} coordination = 4). The ideal, stoichiometric $Cu_2O(111)$ surface is illustrated in Fig. 1a. A nearly-stoichiometric (111) surface can be prepared experimentally by ion bombardment and annealing at 1000 K in vacuum (*17*). The top-layer oxygen-vacancy concentration following such a preparation is estimated at approximately 4% (*16*). An oxygen-deficient $Cu_2O(111)$ surface may also be prepared by exposure to reducing gases. Such treatments lead to a $(\sqrt{3} \times \sqrt{3})R30°$ low-energy electron diffraction (LEED) periodicity due to an ordered one-third of a layer of oxygen vacancies (*17*). Each oxygen vacancy gives rise to a threefold site of singly coordinate Cu^+ cations. The $Cu_2O(111)$-$(\sqrt{3} \times \sqrt{3})R30°$ surface is illustrated in Fig. 1b.

The $Cu_2O(100)$ surface used in this study is a polar, Cu^+-terminated, reconstructed surface which displayed a $(3\sqrt{2} \times \sqrt{2})R45°$ LEED periodicity with many missing spots (*17*). Although there is no definitive model of the structure of the reconstructed surface, the periodicity suggests a relaxation of top atomic layer Cu^+ cations, possibly associated with a weak Cu^+–Cu^+ bonding interaction (*17*). In contrast to the (111) surface, the ideal, Cu^+-terminated (100) surface

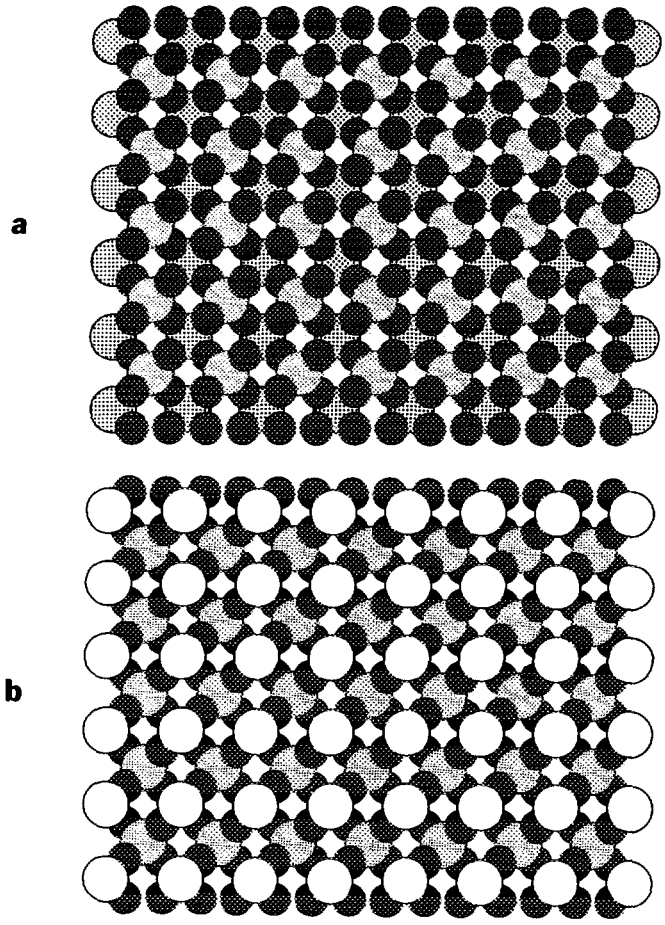

FIG. 2. Ball model illustrations of (a) the ideal (i.e., unreconstructed) Cu^+-terminated (100) surface and (b) the oxygen-terminated (100) surface assuming no relaxation.

exposes no lattice oxygen in the top atomic layer. The top layer Cu^+ cations are singly coordinated. The ideal (i.e., unreconstructed) Cu^+ terminated surface is illustrated in Fig. 2a.

An oxygen-terminated surface can also be prepared by 10^9 L (1 L $\equiv 10^{-6}$ Torr · sec) exposures to O_2 at room temperature. This preparation lifts the reconstruction on the (100) surface to form a (1 × 1), oxygen-terminated surface which is believed to contain doubly coordinate oxygen anions in the outer atomic layer. The oxygen in this terminating layer exhibits electronic properties in photoemission characteristic of incorporated (i.e., lattice) oxygen and adsorbed atomic oxygen (i.e., adatoms) (*17*). This oxygen-terminated (100) surface is shown in Fig. 2b. A more complete description of the characterization of the Cu_2O(100) and (111) surfaces has been reported elsewhere (*17*).

EXPERIMENTAL

All experiments were performed in a dual-chamber, stainless steel, ultrahigh vacuum system equipped for X-ray photoelectron spectroscopy (XPS), LEED, and thermal desorption spectroscopy (TDS). For all thermal desorption experiments the samples were heated linearly at a rate of 2 K/sec.

An Inficon Quadrex 200 was used to monitor up to six masses simultaneously during the thermal desorption experiments. The mass spectrometer was equipped with a quartz skimmer to minimize the sampling of desorption products from the sample support hardware. All TDS traces have been corrected for mass spectrometer sensitivity. The sample preparation and mounting is described in detail elsewhere (*16*).

Dosing was accomplished by exposure of the sample to propene or oxygen at atmospheric pressure in a high pressure cell attached to the vacuum system. The sample rod manipulator passes through sliding seals that separate the UHV system from the high pressure cell. The sample was moved from UHV into the high-pressure cell (in approximately 5 sec), exposed to flowing gas at atmospheric pressure for about 2 sec, then moved back into UHV (in approximately 5 sec). These exposures are referred to as nominally 10^9 L doses. The background pressure was allowed to decrease below 1×10^{-8} Torr prior to the start of a thermal desorption run. Thus, it was possible to dose at atmospheric pressure without exposing the sample to air. The dosing method, while providing easy access to atmospheric pressures, was difficult to control precisely. Significant variations in the amounts of desorbing propene were observed during the TDS experiments due to variations in the total propene dose from run to run. The data shown are representative of the most reproducibly obtained desorption traces.

Matheson polymer-grade propene (99.5%) containing 0.4% propane as the major contaminant was used. Matheson research-grade O_2 (99.997%) was passed through a coiled tube immersed in liquid nitrogen in an attempt to minimize the water content before use.

RESULTS

1. Thermal Desorption: 300 K, 1 atm Exposures

Figures 3–5 show the TDS spectra obtained after a 10^9 L dose of propene at 300 K and 1 atm. on the Cu^+-terminated (100), O-terminated (100), and the (111) surfaces of Cu_2O, respectively. Propene, acrolein, ally alcohol (CH_2=$CHCH_2OH$), propane ($CH_3CH_2CH_3$), CO, CO_2, and H_2O were detected as desorption products from all three surfaces. No bimolecular reaction products were detected (with the exceptions noted below for the (111) surface), and no C_1 or C_2 products were detected besides nonselective oxidation products (CO and CO_2). No H_2 was observed, however, the background pressure of hydrogen in the vacuum system was such that some H_2 may have gone undetected. Since the propene expo-

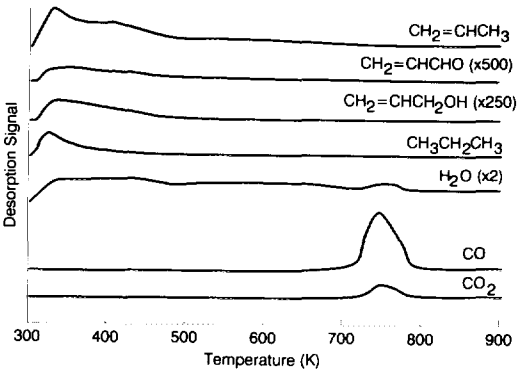

FIG. 3. Thermal desorption traces following a 10^9 L dose of propene at 300 K and 1 atm on the Cu^+-terminated $Cu_2O(100)$ surface.

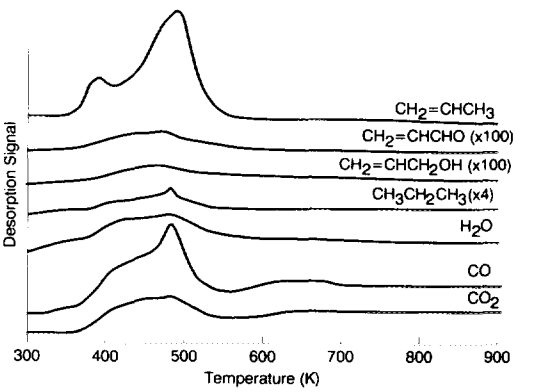

FIG. 4. Thermal desorption traces following a 10^9 L dose of propene at 300 K and 1 atm on the oxygen-terminated $Cu_2O(100)$ surface.

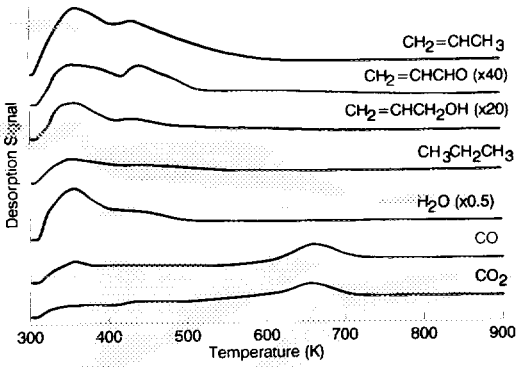

FIG. 5. Thermal desorption traces following a 10^9 L dose of propene at 300 K and 1 atm on the $Cu_2O(111)$ surface.

sures were done in the absence of gas phase oxygen, it is clear that *all oxidation products (selective and nonselective) formed under these conditions utilize lattice oxygen for their formation.* For each surface, the total coverage of propene following a 10^9L exposure was low, with an estimated sticking coefficient on the order of 10^{-10}. The relative product yields from each of the surfaces are given in Table 1. Of the products listed in Table 1, the most difficult to quantify is water. Because the baseline in the thermal desorption experiments is not flat (i.e., it increases with higher temperature) and not linear, the signal vs. time curve cannot be integrated accurately. The variations listed in Table 1 correspond to the range of values attainable by assuming baselines of different shapes.

TABLE 1

Relative Product Yields for 10^9 L Propene Doses at 1 atm and 300 K

Product	Relative yield		
	$Cu_2O(100)$–Cu^+	$Cu_2O(100)$–O	$Cu_2O(111)$
$CH_3CH_2CH_3$	2.5 ± 0.3	0.2 ± 0.1	2.4 ± 0.3
CH_2=$CHCH_2OH$	0.01 ± 0.01	0.03 ± 0.01	0.11 ± 0.02
CH_2=CHCHO	<0.005	0.02 ± 0.01	0.07 ± 0.02
CO	1.7 ± 0.3	1.4 ± 0.3	0.9 ± 0.3
CO_2	1.0 ± 0.3	1.0 ± 0.3	1.0 ± 0.3
H_2O	1.8 ± 0.8	2.0 ± 1.0	4.3 ± 2.3

1.1. Cu^+-terminated $Cu_2O(100)$. Propene desorbs as a broad feature with two peaks at 335 and 400 K (Fig. 3). This temperature range for propene desorption from the Cu^+-terminated (100) surface is similar to the range of 383 to 403 K reported by Mikhal'chenko *et al.* for "reversibly adsorbed" propene on Cu_2O powders (*11*). Acrolein and allyl alcohol both desorb with a peak maximum at 335 K. The coincident desorption of allyl alcohol and acrolein suggests that their evolution involves the same rate-limiting step from a common surface intermediate. The production of CO (*18*) and CO_2 (*19*) at 750 K is reaction-limited. CO and CO_2 peaks in this temperature range have been attributed to the burn-off of adsorbed carbon and hydrocarbon species during studies of C_3 oxygenate decomposition on $Cu_2O(100)$ (*20–22*). Propane desorbs in a single peak with a maximum at 325 K.

H_2O desorbs in a broad feature extending from 325 to 800 K, with small peaks above the background at 335, 420, and 750 K. H_2O thermal desorption studies have shown that the recombination of dissociated water occurs below 460 K (*23*), while studies of predissociated hydrogen adsorption have shown that atomic hydrogen extracts lattice oxygen to form water at 500 K (*24*). Water desorption above 500 K is therefore associated with reaction-limited steps for the dehydrogenation of surface hydrocarbons. The broad temperature range for water desorption suggests that a combination of pathways contribute to water production, and involve rate-limiting steps associated with the disproportionation of surface hydroxyl groups, lattice oxygen extraction by surface hydrogen, and dehydrogenation of surface hydrocarbons.

Propane and propene are the major desorbing species. The conversion of propene following a 10^9 L propene dose is about 43%. The selectivity (calculated on a C_3 basis) is 73% to propane, 16% to CO, 10% to CO_2, 0.3% to allyl alcohol, and less than 0.2% to acrolein. Thus, C_3 oxidation products (allyl alcohol and acrolein) were produced in only

trace amounts from propene on the Cu^+-terminated (100) surface following adsorption at atmospheric pressure and 300 K.

1.2. Oxygen-terminated $Cu_2O(100)$. The propene thermal desorption experiments performed on the Cu^+-terminated (100) surface were repeated on an oxygen-terminated $Cu_2O(100)$ surface to examine the effects of doubly-coordinate surface oxygen on the oxidation of propene. The oxygen-terminated surface was prepared by exposure to 10^9 L of O_2 at 300 K and 1 atmosphere (*17*). The oxygen-terminated surface is stable to less than 500 K in vacuum (*17*), therefore a fresh oxygen-terminated surface was prepared prior to each propene thermal desorption run.

Propene desorbs in a broad feature with a peak at 495 K, and a lower temperature shoulder at 390 K (Fig. 4). The evolution of propene from the oxygen-terminated (100) surface occurs with a desorption temperature nearly 100 K higher than from the Cu^+-terminated (100) surface, illustrating a structure-sensitive interaction for propene adsorption at 300 K under these conditions. Acrolein and allyl alcohol desorb in a single, broad feature with a peak maximum at 480 K. As on the Cu^+-terminated (100) surface, the coincident desorption of allyl alcohol and acrolein suggests that their evolution involves the same rate-limiting step from a common surface intermediate. Propane desorbs as a broad feature extending from 375 to 525 K, with a maximum at 485 K. CO and CO_2 both desorb in a reaction-limited (*18–19*) peak at 485 K. H_2O is also observed at 485 K, in the temperature range expected for water desorption via the extraction of lattice oxygen by surface hydrogen (*23, 24*).

Several changes in the conversion and selectivities of propene to products are observed when comparing the Cu^+-terminated (100) surface with the oxygen-terminated (100) surface. The selectivity (calculated on a C_3 basis) was 19% to propane, 3% to allyl alcohol, 2% to acrolein, 44% to CO, and 32% to CO_2 on the oxygen-terminated surface. The conversion of propene decreased from 43% on the Cu^+-terminated (100) surface to 21% on the oxygen-terminated surface. The selectivity to propane decreased from 73% on the Cu^+-terminated (100) surface to 19% on the oxygen-terminated (100) surface, while the selectivity to oxidation products (both selective and nonselective) increased. The selectivity to acrolein and allyl alcohol rose from a total of less than 0.5% on the Cu^+-terminated (100) surface to 5% on the oxygen-terminated surface, i.e., better than an order-of-magnitude increase.

1.3. $Cu_2O(111)$. All propene TDS experiments were done on an oxygen-deficient $Cu_2O(111)$ surface exhibiting a $(\sqrt{3} \times \sqrt{3})$ R30° LEED pattern (*16, 17*). Trace signals at the detection limits of the mass spectrometer were observed for mass numbers 78 and 67. These signals are attributed to trace amounts of benzene (78) and 1,5 hexadiene (67), but the signals were small enough that an unambiguous identification based on multiple mass numbers in the cracking pattern was not possible. These two compounds are expected as possible bimolecular reaction products of surface allyls. Propene desorbs in one peak at 360 K, with a higher temperature shoulder at 435 K (Fig. 5).

Acrolein and allyl alcohol desorb in two peaks at 350 and 435 K. As on the Cu^+ and oxygen-terminated (100) surfaces, the coincident desorption of allyl alcohol and acrolein suggests that their evolution involves the same rate-limiting step from a common surface intermediate. Propane desorbs in a single feature with a peak maximum at 350 K. CO and CO_2 both desorbed in two reaction-limited peaks (*18, 19*), one coincident with propene at 360 K, and a second higher temperature peak at 660 K. H_2O desorbs in two peaks at 360 and 435 K, which are in the temperature range expected for hydroxyl group disproportionation and extraction of lattice oxygen by atomic hydrogen, respectively (*23, 24*).

The conversion of propene was about 35% for a 10^9 L dose on the (111)-$(\sqrt{3} \times \sqrt{3})$R30° surface at 300 K and 1 atm. The selectivity (calculated on a C_3 basis) to pro-

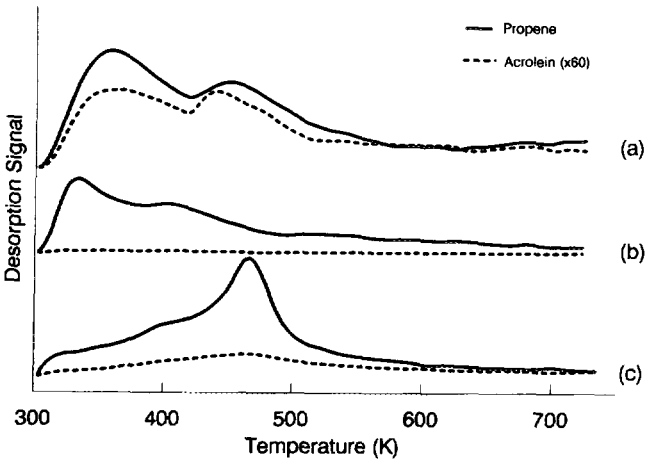

FIG. 6. TDS traces of propene and acrolein following 10^9 L doses of propene at 300 K and 1 atm: (a) $Cu_2O(111)$ surface, (b) Cu^+-terminated $Cu_2O(100)$ surface, and (c) oxygen-terminated $Cu_2O(100)$ surface.

pane was 75%, to CO was 9%, to CO_2 was 10%, to acrolein was 2%, and to allyl alcohol was 3%.

1.4 Structure sensitivity in propene adsorption and acrolein production. For comparison, Fig. 6 shows propene and acrolein TDS traces in a single figure for the three different surfaces described above. Figures 6a–6c show propene (solid lines) and acrolein (dashed lines) desorption from the (111) surface, the Cu^+-terminated (100) surface, and the oxygen-terminated (100) surface, respectively. Note that these data are from different runs than those shown in Figs. 3–5, but still show the same basis characteristics. The differences in the temperatures of the propene desorption states from the three different surfaces clearly demonstrate structure sensitivity for propene adsorption. Specifically, propene from the oxygen-terminated (100) surface desorbs at 480 K for its primary desorption channel, 100 K higher than the primary desorption channel from the (111) and Cu^+-terminated (100) surfaces. The reason for the higher propene desorption temperature on the oxgyen-terminated (100) surface is not understood. Structure sensitivity for propene adsorption has also been observed for adsorption in UHV at low temperature on the $Cu_2O(111)$ surface and the Cu^+-terminated $Cu_2O(100)$ surface (*16*).

Differences in the desorption temperatures and relative amounts of acrolein produced from the different surfaces are also shown in Fig. 6. The acrolein desorption traces (shown as dashed lines) have been scaled to show the true relative yields produced from the different Cu_2O surfaces studied. The relative yield of acrolein from the surfaces varies in the order

$$Cu_2O(111) > Cu_2O(100)\text{–}O > Cu_2O(100)\text{–}Cu^+$$

in typical ratios of 20 : 4 : 1. Thus, the largest acrolein signals are obtained from the two Cu_2O surfaces with readily accessible, coordinately unsaturated surface oxygen in the top atomic layer. The total yield of both selective oxidation products (i.e., acrolein and allyl alcohol) follows a similar pattern.

1.5. Comparison of acrolein desorption signals from different adsorbates. Figure 7 shows acrolein thermal desorption traces originating from several different adsorbates on Cu_2O single-crystal surfaces. The acrolein traces following a 10^9 L exposure of propene (300 K, 1 atm) on the $Cu_2O(111)$ and oxygen-terminated (100) sur-

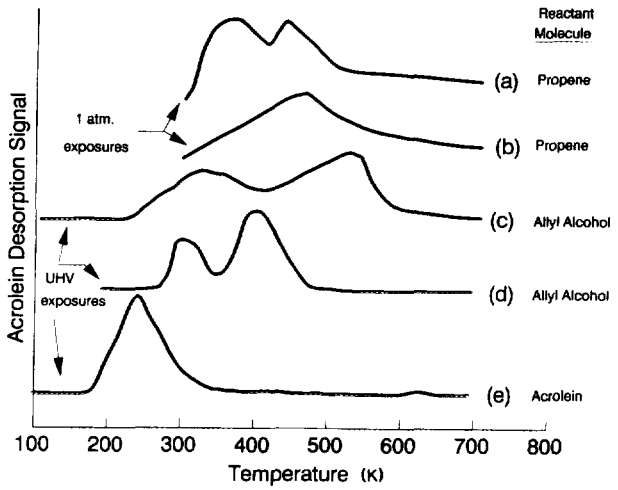

FIG. 7. TDS traces of product acrolein from Cu_2O: (a) acrolein from 10^9 L propene on the $Cu_2O(111)$ surface, (b) acrolein from 10^9 L propene on the oxygen-terminated $Cu_2O(100)$ surface, (c) acrolein from allyl alcohol oxidation on $Cu_2O(100)$, (d) acrolein from allyl alcohol oxidation on $Cu_2O(111)$, and (e) acrolein from TDS of chemisorbed acrolein on $Cu_2O(100)$. All traces have been arbitrarily scaled for comparison.

faces are shown as Figs. 7a and 7b, respectively. These traces have been arbitrarily scaled for comparison. Acrolein TDS traces from both allyl alcohol (0.22 L at 120 K) (*22*) and acrolein (0.25 L at 100 K) (*20*) adsorption studies in UHV on the Cu^+-terminated (100) surface at low temperature are shown as Figs. 7c and 7e, respectively. An acrolein trace from allyl alcohol decomposition on the $Cu_2O(111)$ surface (3 L at 120 K) is shown in Fig. 7d. By comparison to the desorption signal from a molecular acrolein adsorbate, it is seen that the desorption of acrolein from the allyl alcohol and propene exposures is reaction-limited. The similarity in desorption temperatures of the acrolein peaks from allyl alcohol adsorption in UHV on the Cu^+-terminated (100) and (111) surfaces and the acrolein peaks from 1 atm propene exposures suggests that the rate-limiting steps involve the same surface intermediates.

2. *XPS*

2.1. $Cu_2O(100)$. XPS was used to investigate the surface species resulting from propene adsorption at 300 K and 1 atm on the $Cu_2O(100)$ surface to check for the formation of an oxygen-containing σ-allyl. A C 1*s* peak broadened to higher binding energies would be expected for an oxygen-containing surface intermediate because of the electron withdrawing nature of oxygen (*20–22, 25*). For the XPS experiments, 10^9 L exposures of propene on both the Cu^+-terminated and oxygen-terminated (100) surfaces at 300 K were examined. The resulting C 1*s* XPS spectra are shown in Fig. 8.

The C 1*s* spectrum of the Cu^+-terminated (100) surface is shown in Fig. 8a. One peak was fit to this spectrum at a binding energy of 284.9 ± 0.1 eV and a FWHM of 1.6 eV. This binding energy (284.9 eV) is characteristic of adsorbed hydrocarbons (i.e., propene, alkyl carbons, vinyl carbons, etc.) on Cu_2O (*16*). No broadening of the C 1*s* XPS spectrum to higher binding energy was observed, illustrating that oxygen insertion does not occur *to an extent detectable with XPS*. This result is consistent with the thermal desorption data which showed that less than 0.2% of the adsorbed propene is converted to C_3 oxidation products.

Figure 8b shows the C 1*s* spectrum of

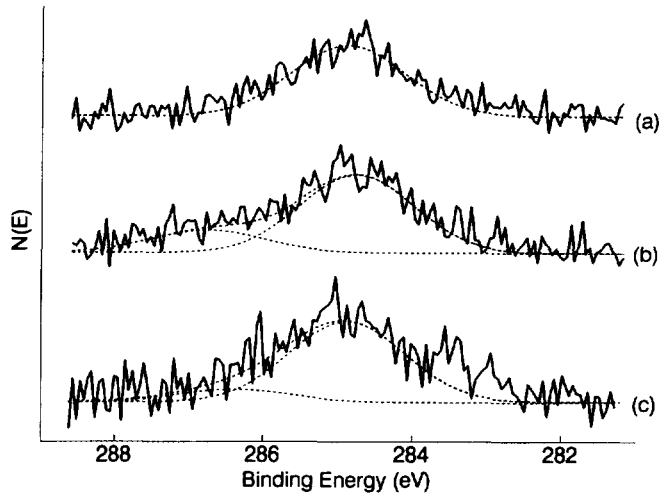

FIG. 8. C 1*s* XPS spectra of 10^9 L of propene on $Cu_2O(100)$ and (111): (a) propene adsorbed on the Cu^+-terminated (100) surface, (b) propene adsorbed on the oxygen-terminated (100) surface, and (c) propene adsorbed on the $Cu_2O(111)$ surface.

10^9 L of propene adsorbed on the oxygen-terminated (100) surface. This spectrum is broadened to higher binding energy, characteristic of the formation of an oxygen-containing surface species following propene adsorption. Two contributions are observed at binding energies of 286.8 ± 0.1 and 284.9 ± 0.1 eV. The peak at 286.8 eV is near the binding energy expected for the oxygenated carbon of a surface alkoxide species (286.4 eV) (*22*).

Previous studies of propene oxidation over Cu_2O have suggested the formation of an oxygen-containing σ-allyl species in the propene oxidation pathway (*1–3*). The presence of an alkoxide species in XPS and the occurrence of acrolein as a thermal desorption product are consistent with the formation of an oxygen-containing, σ-allyl species following propene adsorption at 300 K and 1 atm. Thus, the species which give rise to the C 1*s* XPS peak at 286.6 eV is assigned to the oxygenated carbon of an oxygen-containing σ-allyl.

2.2. $Cu_2O(111)$. Figure 8c shows the C 1*s* spectrum following a 10^9 L propene dose on the (111) surface at 300 K and 1 atm. Two contributions are found to this spectrum at binding energies of 284.9 ± 0.1 and 286.4 ± 0.1 eV. Similar to the oxygen-terminated (100) surface, the peak at 286.4 eV is at the binding energy expected for the oxygenated carbon of a surface alkoxide species (286.4 eV) (*22*). This XPS feature is *not* characteristic of the bound formyl group of an aldehydic species (287.2 eV) on this surface (*20*). The peak at 286.4 eV is assigned to the oxygen-containing σ-allyl. Thus, evidence for oxygen insertion leading to the formation of an oxygen-containing σ-allyl is observed in XPS for both the (111) and the oxygen-terminated (100) surfaces.

DISCUSSION

1. Comparison of Propene Adsorption at Low Pressure and 1 atm

Both differences and similarities were observed between propene adsorption in vacuum and at atmospheric pressure. The desorption temperatures of propene following either low pressure or atmospheric pressure adsorption at 300 K were similar for the (111) and Cu^+-terminated (100) surfaces. Propene desorbs at 315 K after a 3000 L dose at 10^{-4} Torr on the Cu^+-terminated (100) surface, and at 360 K from the (111) surface

(*16*). The primary desorption channel following a 10^9 L propene dose at atmospheric pressure is 335 K for the Cu^+-terminated (100) surface, and 360 K for the (111) surface, similar to the values reported for propene adsorption at 10^{-4} Torr (*16*). Propene adsorption (3000 L at 10^{-4} Torr) was also studied on a $Cu_2O(100)$ surface predosed with 0.3 ML of atomic oxygen (*16*). The primary propene desorption channel from this surface was at 315 K, 180 K lower than the primary propene desorption channel (495 K) from the oxygen-terminated (100) surface following a 1 atm exposure.

Several differences were observed between the propene reactivity for low-pressure and 1 atm exposures at 300 K. First, no selective or non-selective oxidation products were observed for propene adsorption in vacuum with the exception of trace amounts of CO from the (111) surface (*16*). Thus, no evidence of *selective* oxygen insertion was observed under any conditions for propene adsorption at 300 K with exposures up to 3000 L at pressures of 10^{-4} Torr or less. The presence of an oxygen-containing σ-allyl species following a 10^9 L (1 atm) propene dose on either the oxygen-terminated (100) or the (111) surfaces gives clear evidence that oxygen insertion takes place at higher pressure as demonstrated by XPS and the observation of acrolein and allyl alcohol in TDS. Second, no hydrogenation activity was observed on either the (100) or (111) surfaces for propene adsorption in vacuum. Indeed, no propane was formed even for propene adsorption on hydrogen-predosed surfaces in vacuum. Thus, clear differences in the reactivity of propene were observed for exposures in vacuum and at atmospheric pressure, suggesting a "pressure gap" exists between the low pressure and atmospheric pressure chemistry.

The origin of the "pressure gap" in catalysis has been addressed recently for methane activation on nickel (*26*). For methane adsorption on Ni(111), dissociation is observed for pressures above 1 Torr, but no dissociation is observed below 10^{-4} Torr (*26*). Ceyer and co-workers found that the pressure dependence for CH_4 dissociation on Ni is related to the presence of an energy barrier along the dissociative reaction coordinate (*26*). Only those molecules with sufficient translational energy overcome the barrier to dissociation. An increase in pressure increases the absolute number of gas-phase molecules with translational energy sufficient to overcome this barrier.

Similar processes could explain the differences in chemistry observed between the UHV and 1 atm. exposures of propene at 300 K over Cu_2O surfaces. In the UHV work (*16*), dissociative adsorption of propene to allyl was observed with a sticking coefficient of less than 10^{-5}. Since no selective oxidation products were observed, it appears that the propene "activation" process involves not just the initial dissociation to a π-allyl, but also the separate process of oxygen insertion. The reaction probability for such events at 300 K is far below 10^{-5}. The clear observations of oxygen-containing surface species and subsequent selective oxidation following exposures at 300 K and 1 atm strongly suggests that oxygen insertion to form a σ-allyl can be accomplished via processes such as translational or collisional activation (*26*). Additionally, for a molecule as large as propene, vibrational excitations may also play a role in surmounting the barrier to propene "activation."

As mentioned above, propene dissociation to an allylic species was observed for 3000 L doses at 300 K in vacuum (*16*). The presence of the hydrogenation product (propane) following a 10^9 L propene exposure at 1 atm, which was not observed for propene adsorption in vacuum suggests two possibilities for the differences in reactivity. The first possibility is that desorption of the reactants adsorbed in vacuum occurs in TDS with a lower activation energy (and hence at a lower temperature) than required to hydrogenate the allylic surface species. Adsorption at atmospheric pressure could facilitate the reaction by translational and collisional activation to surmount the bar-

rier to hydrogenation. The second possibility is that propene adsorption at atmospheric pressure gives rise to a propane-yielding surface intermediate different from the allylic species obtained by adsorption in vacuum. Possible examples include the formation of a surface propylidyne species ($CH_3CH_2C\equiv$) such as that observed for propene adsorption on Pt(111) and Rh(111) surfaces (*27, 30*), or the disproportionation of propene to allyl and propyl radicals which, if not a highly activated process, might be kinetically favored at the higher propene coverages at 1 atm. Labeling experiments were attempted where the Cu_2O surfaces were first predosed with atomic deuterium then exposed to propene at atmospheric pressure. It was anticipated that the maximum number of deuterium atoms incorporated into the propane product would indicate the number of carbon-surface bonds of the propane intermediate, e.g., three for a propylidyne or one for a surface propyl radical. However, no clear signal from deuterium-labeled propane of any kind was observed. Unfortunately, such experiments involving atmospheric pressure exposures are much less clean and well-controlled than vacuum experiments. No identification of the surface intermediate leading to propane can be made from the available experimental data.

The source of hydrogen for propane formation is believed to be the hydrogen released from dissociative propene adsorption and oxidation. The relative product yields from the two (100) surfaces show that the hydrogen material balance closes, at least within the limits of error on the measurements. On the (111) surface, propene oxidation provides enough hydrogen to account for the propane (again within the limits of error), but not the water. As stated previously, the water was the most difficult species to quantify. The possibility of some water adsorption during the propene exposures is also recognized. For the large doses (10^9L) used, even an undetectable 1 in 10^8 parts water contamination could give an amount of adsorbed water detectable by TDS. However, the uptake of water by dissociative adsorption at 300 K is limited on Cu_2O surfaces. For example, on the (100)-Cu^+ surface, the uptake of water at 300 K is limited to about 10% of a ML (*23*). By comparison to the previous water TDS study, the total amount of water desorbed following a 10^9L propene exposure varies from about 0.03 to 0.07 ML. Run to run variations for a given surface fall within this range, but the amount of desorbed water does not correlate directly with the amounts of oxidation products formed. Hence, any such small amount of contaminant water that may be adsorbed does not significantly effect the selective or nonselective oxidation processes.

2. *Allyloxy: Key Intermediate for Acrolein Formation*

UHV thermal desorption studies of the reaction of allyl alcohol with the $Cu_2O(100)$ surface have shown that product acrolein is formed from an allyloxy ($CH_2{=}CHCH_2O{-}$) surface intermediate via a rate-limiting, first-order, unimolecular, hydride elimination from the carbon α to the oxygen heteroatom (*22*). As reported previously (*22*) and illustrated in Fig. 7c, this rate-limiting step occurs at 525 K on the Cu^+-terminated (100) surface (i.e., the high-temperature desorption feature in Fig. 7c) with a corresponding activation energy of 35.6 kcal/mole (*22*). The characteristic signature of this reaction is the concurrent desorption of allyl alcohol (not shown in Fig. 7, see Ref. (*22*)) with acrolein by recombination of allyloxy with surface hydrogen at the same temperature. Both species appear at the same temperature because the hydride elimination step is rate-limiting for the evolution of both molecules. The corresponding results for acrolein production from allyl alcohol on $Cu_2O(111)$ shown in Fig. 7d (previously unreported) are explained by the same chemical process. Specifically, the highest temperature acrolein desorption signal at 400 K in Fig. 7d is assigned to allyloxy decomposi-

tion for the same reasons described above and in Ref. (*22*). Assuming a normal, first-order pre-exponential (10^{13} sec^{-1}) and applying the Redhead equation (*31*) gives an activation energy of 26.9 kcal/mole for allyloxy decomposition to acrolein on $Cu_2O(111)$. A lower temperature acrolein desorption pathway proposed to involve an enolate intermediate produced from allyloxy has also been observed at 310 K on the (100) surface (*22*) and 300 K on the (111) surface as evidenced by the low-temperature acrolein desorption features in Figs. 7c and 7d.

For atmospheric pressure exposures of propene on the $Cu_2O(111)$ and oxygen-terminated (100) surfaces, acrolein is evolved at 435 K (29.4 kcal/mole) and 480 K (32.5 kcal/mole), respectively. Comparison with the desorption trace of adsorbed acrolein in Fig. 7d shows clearly that the acrolein produced from propene is reaction-limited and falls within the range of temperatures and activation energies observed for the structure-sensitive allyloxy decomposition kinetics on the (111) and (100) surfaces. The concurrent desorption of allyl alcohol is also confirmed in Figs. 4 and 5 following atmospheric pressure propene exposures. Hence, the production of acrolein from propene clearly involves an allyloxy intermediate rather than an aldehydic (i.e., acrolein-like) intermediate. Some acrolein production from propene is even observed at 350 K, similar to the proposed enolate-mediated route for allyloxy decomposition (*20*).

The assignment of acrolein production from an allyoxy surface intermediate in propene oxidation is also consistent with the C 1*s* XPS data for adsorbed propene. The binding energy for the oxygen-containing σ-allyl species is consistent with the binding energy observed for allyloxy species on $Cu_2O(100)$ (*22*). The production of acrolein via an allyloxy surface intermediate demonstrates that oxygen insertion occurs *before* the second hydrogen abstraction in the propene oxidation pathway. Additionally, studies of the reaction of preadsorbed hydrogen with acrolein on $Cu_2O(100)$ have shown that hydrogenation of an aldehydic (acrolein-like) species to an allyloxy does not occur to a significant extent (*20*). Thus, the coincident desorption of allyl alcohol and acrolein demonstrate that an aldehydic or acrolein-like intermediate (expected if the second hydrogen abstraction precedes oxygen insertion) is not responsible for the observed allyl alcohol or acrolein from propene on Cu_2O.

Adams and Jennings studied the oxidation of various deuterated propenes over Cu_2O (*4*). They observed a kinetic isotope effect in the formation of acrolein from deuterated propenes, and concluded that removal of the second hydrogen from a π-allyl occurs prior to oxygen insertion. Their labeling experiments clearly test which of the last two reaction steps after the initial dissociation to a π-allyl (i.e., the second hydrogen abstraction or the oxygen insertion) is rate limiting. However, their interpretation of the primary kinetic isotope effect involves the unstated but clear assumption that the first of these two remaining steps (i.e., the initial attack of the π-allyl intermediate) will be the slowest. Note, however, that while the primary kinetic isotope effect demonstrates that hydrogen abstraction is the slower of these last two steps, it *does not* indicate the relative order in which these two final steps occur. Our results show clearly that of these last two reaction steps the first-order, unimolecular, hydride elimination from the carbon α to oxygen in a surface allyloxy (which occurs between 400 and 525 K in TDS) is rate-limiting. However, the oxygen insertion reaction clearly occurs first, as evidenced by the presence of a signal due to a stable alkoxide (allyoxy) species in XPS following propene adsorption at 300 K. Thus, our data and interpretation are consistent with the data of Adams and Jennings, although we draw the opposite conclusion. In summary, of the last two reaction steps, the initial attack of lattice oxygen on the symmetric π-allyl intermediate is the fastest (occurring at atmospheric pressure and 300

K). The subsequent hydride elimination from the stable allyoxy species is the slower of these two steps, occurring at temperatures above 300 K in TDS.

3. *Role of Surface Oxygen in Propene Oxidation*

One of the most widely accepted general principles in the area of the selective oxidation of hydrocarbons over metal oxides is that lattice oxygen (O^{2-}) is responsible for selective oxidation while adsorbed oxygen (both molecular and atomic in various charge states) is responsible for the nonselective formation of carbon oxides (*32*). The role of lattice versus adsorbed oxygen in the formation of acrolein from propene over different oxide surfaces has been investigated specifically (*33*, *34*). Akimoto *et al.* studied propene oxidation over Cu_2O catalysts with $^{18}O_2$ as an oxidant and concluded that adsorbed oxygen was incorporated into acrolein, not lattice oxygen (*33*). In contrast, Keulks studied propene oxidation with $^{18}O_2$ over bismuth–molybdate catalysts, and suggested that lattice oxygen, not adsorbed oxygen, was incorporated into acrolein (*34*). However, our results over Cu_2O single-crystal surfaces involving propene adsorption with no oxygen cofeed demonstrate that lattice oxygen is incorporated into *all* the oxidation products (selective and nonselective) observed under the conditions of our study. While it may be reasonable to describe one particular form of oxygen as being the primary oxidant participating in the formation of a certain product, our results demonstrate specifically that lattice oxygen, O^{2-}, in Cu_2O can be involved in both selective and non-selective processes.

The use of the Cu^+-terminated (100), oxygen-terminated (100), and (111) Cu_2O single-crystal surfaces allows for the testing of oxygen-related site requirements for propene selective oxidation. While it is recognized that the overall production of selective oxidation products in our TDS measurements depends on both the selectivity for allyoxy formation and decomposition, the similar selectivities for these products (acrolein and allyl alcohol) *and* the observation of an oxygenated surface intermediate in XPS for both the oxygen-terminated (100) and (111) surfaces demonstrates that the selective insertion of lattice oxygen occurs with both two-coordinate (from the oxygen-terminated (100)) and three-coordinate surface oxygen anions (from the (111) surface). The lower yields and selectivities for the formation of selective oxidation products and the lack of an observable oxygenated intermediate in XPS for the Cu^+-terminated (100) surface suggests that coordinately-saturated lattice oxygen is much less efficient for the selective oxygen insertion reaction. These observations suggest that the selective insertion reaction over Cu_2O is well-described by a site requirements involving predominantly coordinately *unsaturated* surface lattice oxygen. We note, however, that the role of adsorbed oxygen (as opposed to lattice oxygen) has not been effectively addressed in our studies. In summary, there is no clear correlation between the coordination number of coordinately unsaturated oxygen and the formation of selective oxidation products on Cu_2O; both two and three-coordinated oxygen gives rise to selective oxidation products.

For the nonselective oxidation pathway, CO and CO_2 production under our experimental conditions occurs via burnoff of surface carbon at high temperature from the Cu^+-terminated Cu_2O(100) surface where all the oxygen is fully coordinate (i.e., four-coordinate), subsurface, second-atomic layer, lattice oxygen. In addition, however, lower-temperature nonselective oxidation pathways are available in the presence of coordinately unsaturated lattice oxygen on the (111) and oxygen-terminated (100) surfaces. In particular, the yield and selectivity to carbon oxides are highest from the oxygen-terminated Cu_2O(100) surface (doubly coordinate surface oxygen) with the majority of CO and CO_2 formed below the high-temperature burnoff reaction. Hence, the

two-coordinate surface oxygen on the oxygen-terminated (100) surface most readily forms carbon oxides in comparison to the three-coordinate and four-coordinate forms on the other surfaces. Under our experimental condition, however, this nonselective oxidation occurs primarily at the expense of the reduction process which forms propane, rather than the selective oxidation process which forms acrolein and allyl alcohol.

While surface-dependent variations in selective and nonselective oxygen insertion can be observed from the thermal desorption data, effects of surface conditions on the initial dissociation of propene are less pronounced. In studies of propene adsorption on Cu_2O single crystal surfaces in UHV at low temperatures ($\leq$120 K), it was found that only the Cu_2O(111) surface was capable of dissociating propene (*16*). However, our results following propene adsorption at 1 atm and 300 K agree with those for adsorption at 300 K and intermediate pressures ($P \approx 10^{-4}$ Torr) (*16*). Under these conditions of higher temperature and pressure, the dissociative adsorption of propene is observed on the both oxygen and Cu^+-terminated (100) surfaces as well as the (111) surface. These results suggest that the probability for propene dissociation at 300 K is reasonably independent of the available surface sites (i.e., a structure-insensitive reaction) since it only varies by about a factor of 2. As with the reactivity differences observed between high and low pressure, this dissociation of propene at 300 K is likely controlled by translational and collisional activation processes, rather than the energetic differences associated with structural and compositional differences in the surfaces.

4. *Reversibility in the Selective Oxidation Pathway*

In earlier studies, propene production via a facile, low-temperature reaction (160 K) has been observed during allyl alcohol thermal desorption experiments (*22*). This low-temperature (160 K) pathway has been assigned to the deoxygenation of surface allyloxy to form a resonance-stabilized π-allyl species (*22*). The formation of propene via a low temperature facile reaction through a π-allyl is consistent with previous studies of propene oxidation over Cu_2O which have demonstrated that propene dissociates to form a symmetric, π-allyl species (*4, 8*) prior to oxygen insertion. The results described above demonstrate that propene oxidation occurs through an allyloxy intermediate on Cu_2O as clearly indicated by the formation of allyl alcohol as a selective oxidation product. Thus, the combination of the allyl alcohol and 1 atm. exposure propene thermal desorption results suggest that the pathway from propene to a π-allyl species to an allyloxy species (i.e., oxygen-containing σ-allyl) is reversible on Cu_2O.

Imachi *et al.* have previously suggested that no interconversion from a σ-allyl to a π-allyl takes place under reaction conditions in propene oxidation over Cu_2O (*13*). They base this conclusion on kinetic isotope results which suggests that the different allylic species are not in equilibrium. While our data do not address an equilibrium situation, the lack of equilibrium between the π- and σ-allyls is consistent with our results and interpretation of the chemistry over Cu_2O. The stability of the allyloxy to temperatures of over 400 K, and the facile, low-temperature reaction to propene thought to be associated with a π-allyl suggests recombination of π-allyl to propene proceeds at a much faster rate under our reducing conditions (no oxygen cofeed) than the decomposition of allyloxy (σ-allyl), thus leading to kinetic rather than equilibrium control of the concentrations of π- and σ-allyls. The observation of propene as a reaction product from allyl alcohol (*22*) provides evidence that the reaction pathway between π- and σ-allyls is reversible, if not at equilibrium. In related work over Cu_2O, Choi *et al.* (*9*) report unexplained oxygen scrambling from ^{18}O-labeled allyl alcohol to give labeled and unlabeled acrolein product. We suggest that these observations are also

evidence for the reduction of the σ-allyl with subsequent reoxidation, consistent with a reversible pathway for the conversion of π- to σ-allyl.

CONCLUSIONS

Propene oxidation was studied on Cu_2O single-crystal surfaces using XPS and TDS with propene exposures at 300 K and atmospheric pressure. Three different Cu_2O surfaces were examined: a Cu^+-terminated (100) surface, an oxygen-terminated (100) surface, and a (111) surface with accessible copper cations and lattice oxygen. Clear structure sensitivity in the interaction of propene with Cu_2O was observed by differences in the desorption temperatures of propene from each of the three surfaces studied. Propene dissociation at 300 K, however, appears to be independent of the available surface sites on Cu_2O, but the selective oxidation to acrolein is promoted by coordinately unsaturated surface lattice oxygen. No clear correlation between the formation of partial oxidation products and oxygen coordination was observed, but two coordinate surface oxygen on the oxygen-terminated (100) surface was found to promote nonselective oxidation at the expense of the hydrogenation reaction to propane. Under the experimental conditions described here, both the selective and nonselective oxidation products are formed from lattice oxygen.

The propene oxidation pathway was shown to proceed through an allyloxy (CH_2=$CHCH_2O$–) species where oxygen insertion occurs prior to the second hydrogen abstraction over Cu_2O. This conclusion was reached by comparison of propene TDS results from atmospheric pressure exposures with UHV allyl alcohol and acrolein thermal desorption studies. The production of propene from allyl alcohol demonstrates that the formation of the oxygen-containing, σ-allyl (allyloxy) species is reversible on Cu_2O. The selective oxidation process over Cu_2O is subject to a "pressure gap" at 300 K with oxygen insertion occurring at higher pressures, presumably because of translational and collisional activation. However, the subsequent steps in the selective oxidation pathway can be effectively modeled by dissociative adsorption of oxygenates under UHV to simulate the oxygenated surface intermediates.

ACKNOWLEDGMENTS

We gratefully acknowledge the National Science Foundation for support of this work through CBT-870876. We also thank Professor M. Tapiero for providing the single crystal used in this study.

REFERENCES

1. Keulks, G. W., Krenzke, L. D., and Noterman, T. M., *Adv. Catal.* **27,** 183 (1978).
2. Hucknall, D. J., "Selective Oxidation of Hydrocarbons." Academic Press, New York, 1974.
3. Grasselli, R. K., and Burrington, J. D., *Adv. Catal.* **30,** 133 (1981).
4. Adams, C. R., and Jennings, T. J., *J. Catal.* **3,** 549 (1964).
5. Grasselli, R. K., and Suresh, D. D., *J. Catal.* **25,** 273 (1972).
6. Godin, G. W., McCain, C. C., and Porter, E. A., *in* "Proceedings, 4th International Congress on Catalysis, Moscow, 1968" (B. A. Kazansky, Ed.), Vol. 1, p. 271. Adler, New York, 1968.
7. Adams, C. R., and Jennings, T. J., *J. Catal.* **2,** 63 (1963).
8. Voge, H. H., Wagner, C. D., and Stevenson, D. P., *J. Catal.* **2,** 58 (1963).
9. Choi, H.-S., Lin, J.-T., and Kuczkowski, R. L., *J. Catal.* **99,** 72 (1986).
10. Mikhal'chenko, V. G., Sokolovskii, V. D., Filippova, A. A., and Davydov, A. A., *Kinet. Katal.* **14,** 1253 (1973).
11. Mikhal'chenko, V. G., Sokolovskii, V. D., and Boreskov, G. K., *Kinet. Katal.* **14,** 698 (1973).
12. Davydov, A. A., Mikhal'chenko, V. G., Sokolovskii, V. D., and Boreskov, G. K., *J. Catal.* **55,** 299 (1978).
13. Imachi, M., Kuczkowski, R. L., Groves, J. T., and Cant, N. W., *J. Catal.* **82,** 355 (1983).
14. Wood, B. J., Wise, H., and Yolles, R. S., *J. Catal.* **15,** 355 (1969).
15. Gorokhovatskii, Ya. B., Vovyanko, I. I., and Rubanik, M. Ya., *Kinet. Katal.* **7,** 76 (1966).
16. Schulz, K. H., and Cox, D. F., *Surf. Sci.* **262,** 318 (1992).
17. Schulz, K. H., and Cox, D. F., *Phys. Rev. B.* **43,** 1610 (1991).
18. Cox, D. F., and Schulz, K. H., *Surf. Sci.* **249,** 138 (1991).
19. Schulz, K. H., and Cox, D. F., unpublished. Ther-

mal desorption studies of CO_2 have shown that all CO_2 desorbs below 300 K on $Cu_2O(100)$.

20. Schulz, K. H., and Cox, D. F., *J. Phys. Chem.* **97,** 3555 (1993).
21. Schulz, K. H., and Cox, D. F., *J. Phys. Chem.* **96,** 7394 (1992).
22. Schulz, K. H., and Cox, D. F., *J. Phys. Chem.* **97,** 647 (1993).
23. Cox, D. F., and Schulz, K. H., *Surf. Sci.* **256,** 67 (1991).
24. Schulz, K. H., and Cox, D. F., *Surf. Sci.* **278,** 9 (1992).
25. Wagner, C. D., Riggs, W. M., Davis, L. E., Moulder, J. F., and Muilenberg, G. E., "Handbook of X-Ray Photoelectron Spectroscopy." Perkin–Elmer, Eden Prairie, MN, 1978.
26. Ceyer, S. T., *Langmuir* **6,** 82 (1990).
27. Salmeron, M., and Somorjai, G. A., *J. Phys. Chem.* **86,** 341 (1982).
28. Koestner, R. J., Frost, J. C., Stair, P. C., Van Hove, M. A., and Somorjai, G. A., *Surf. Sci.* **116,** 85 (1982).
29. Gavezotti, A., Simonetta, M., Van Hove, M. A., and Somorjai, G. A., *Surf. Sci.* **122,** 292 (1982).
30. Koestner, R. J., Van Hove, M. A., and Somorjai, G. A., *J. Phys. Chem.* **87,** 203 (1983).
31. Redhead, P. A., *Vacuum* **12,** 203 (1962).
32. Bielanski, A., and Haber, J., *Catal. Rev.-Sci. Eng.* **19,** 1 (1979).
33. Akimoto, M., Akiyama, M., and Echigoya, E., *Bull. Chem. Soc. Jpn.* **49,** 3367 (1976).
34. Keulks, G. W., *J. Catal.* **19,** 232 (1970).